Appraisal of Fluid Dynamic Efficiency of Retreated-Blade and Turbofoil Impellers in Industrial-Size CSTRs

Marina Campolo and Alfredo Soldati*

Centro Interdipartimentale di Fluidodinamica e Idraulica and Dipartimento di Scienze e Tecnologie Chimiche, Università di Udine, 33100 Udine, Italy

In this work, we examine the performances of two different impellers produced for glass-lined industrial vessel installations. Starting from an experimental evaluation of the power number−Reynolds number curve, we exploit fully three-dimensional, time-dependent fluid dynamic simulations to identify the optimal operating conditions for the widely used retreated-blade impeller and the newer turbofoil turbine. We calculate the power consumption, stirring capability, and pumping efficiency with the final aim of finding guidelines to select the best impeller/vessel configuration. Results show that the turbofoil turbine is more efficient than the retreated-blade impeller in terms of pumping capability and pumping efficiency for operating conditions corresponding to Reynolds numbers larger than 3000. A detailed description of the fluid dynamic field is used to explain and justify the macroscopic evidence.

1. Introduction

Glass-lined vessels, widely used in the chemical and pharmaceutical industries, are usually equipped with retreated curved-blade impellers (retreated-blade impellers). The reasons are mostly technological. The rounded shape of this traditional type of impeller eases glass lining,[1] and in addition, the customarily torospherical shape of the bottom of industrial vessels allows this impeller to be placed very close to the bottom, making this impeller/tank configuration very efficient for suspending heavy dispersions. However, because different types of impellers might suspend more efficiently, and because new technologies allow for the manufacture of more complex glass shapes, we decided to analyze the fluid mechanical efficiency of two different industrial-scale impeller/tank configurations with the object of optimizing the mixing and the mixing time.[2] We used accurate numerical simulations, as extensive experimental investigations of industrial reactors are too costly. In a previous work,[3] we set up an accurate numerical procedure for examining the fluid mechanics of an industrial-size reactor of 12 500-L nominal capacity equipped with a retreated curved-blade impeller (RCBI). In that work, we focused first on a scale replica (440:1 volume ratio) of the reactor and validated the fluid dynamics simulations against original experimental data. Then, by comparing the simulations on the small and industrial scales, we could establish scaling procedures.

In this work, our objective is to compare the fluid mechanical efficiency of an industrial-size reactor equipped with a RCBI against that of the same reactor equipped with a turbofoil turbine (TT) in the operating range of Reynolds numbers from laminar to fully turbulent flow. We use fully transient and three-dimensional computational fluid dynamic simulations, and we start from experimental evidence—an industrial measurement—and from the power number−Reynolds number empirical curve of Nagata.[4] We examine the macroscopic indicators of fluid mechanical efficiency—pumping capability, power consumption, and pumping efficiency—and identify the optimal range of Reynolds number for both impellers. Finally, we justify the different performances of the two impellers from a microscopic fluid mechanical analysis.

* Corresponding author. E-mail: soldati@uniud.it. Phone: 0432-558864. Fax: 0432-558803. Internet: http://158.110.50.22.

2. Methodology

The reactor under investigation has a nominal capacity of 12 500 L, is glass-lined, has a torospherical bottom, and is equipped with two beaver-tail baffles to improve the top−bottom turnover. We investigated the behavior of the reactor equipped with a RCBI and with a TT using a finite-volume commercial code (StarCD) that solves for the balance equations of mass and momentum in Reynolds-averaged form. The geometries of the vessel equipped with the RCBI and with the TT are shown in Figure 1, and all relevant dimensions are presented in Table 1. To solve numerically the balance equations for the fluid in the vessel and to characterize the fluid dynamics of the CSTR, we discretized the volume of the tank into finite volumes, taking care in refining the mesh in the regions where the velocity spatial gradients are expected to be large, i.e., in the impeller region and in the baffle region. The different geometries of the impeller influenced the discretization. For the RCBI configuration, we used 136 592 finite volumes, which ensured an accurate comparison with measurements and a semiempirical curve.[3] For the TT configuration, we used 327 278 finite volumes, which were necessary to reproduce (i) the curvature of the blades, which is variable with distance from the rotation axis, and (ii) the finite blade thickness. The dimensions of the finite volumes were shrunk down to 0.025 m, corresponding to the blade thickness in the impeller region, and volumes of comparable dimensions were also used in the part of the tank below the impeller. Preliminary runs ensured that the mesh was sufficiently refined to yield grid-independent results.

Because the position of the baffles relative to the impeller changes continuously while the impeller rotates, the flow field in the tank changes continuously

10.1021/ie010561e CCC: $22.00
Published on Web 02/08/2002

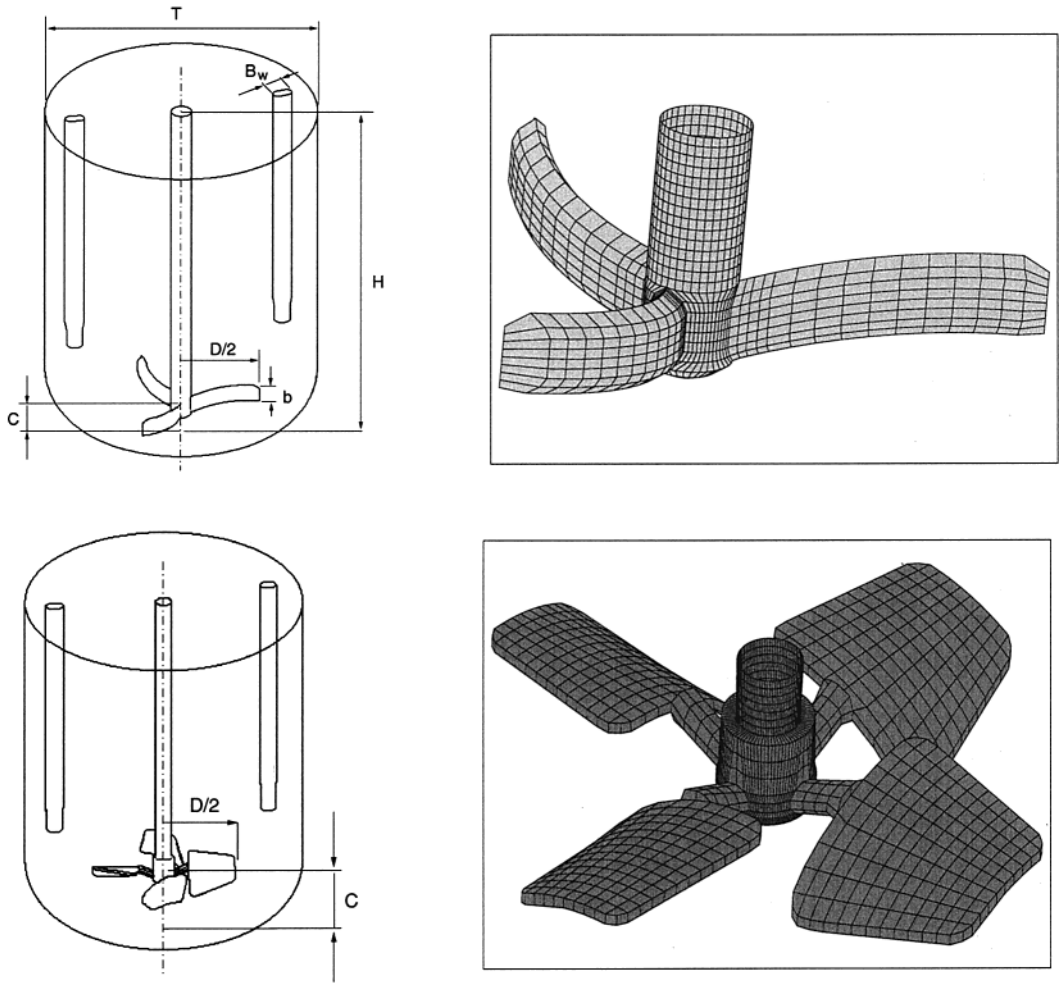

Figure 1. Vessel equipped with RCBI (top) and TT (bottom) and closeup of impeller shapes. Rotation of the impellers is counterclockwise.

Table 1. Geometrical Dimensions of Vessel and Impellers for Industrial Installation

Vessel Data		
tank diameter	T	2.348 m
liquid height	H	3.10 m
baffle width	B_w	0.17 m
number of baffles	n_B	2

Impeller Data			
		RCBI	TT
impeller diameter	D	1.35 m	1.2 m
impeller clearance	C	0.260 m	0.517 m
blade width	b	0.17 m	0.265−0.476 m
number of blades	n_b	3	4
blade inclination[a]	θ	90°	30°

[a] Inclination is measured from a horizontal plane.

through time. To capture the relevant fluid mechanical effects, we solved the balance equations for the fluid using a transient, sliding-mesh approach based on calculating the flow field at each incremental position of the impeller. The sliding-mesh approach involves the use of two computational subgrids: (i) one around the impeller (rotating region), comprising 46 152 cells for the RCBI configuration and 133 384 cells for the TT configuration, and (ii) one for the rest of the vessel (static region). A rotating frame of reference and a stationary frame of reference are used in turn to solve the fluid equations in regions i and ii. The boundary conditions set on the surface of the cells adjacent to the two regions are updated at each incremental time step. The computation starts from the initial condition of fluid at rest in the entire domain, and the flow field is allowed to evolve as driven by the impeller until a pseudo-steady state is attained. This method appears to be the natural method for simulating the flow field in a CSTR, and yet, because of its computational requirements, which involve long transients, highly refined grids, and robust computational techniques, we are not aware of many examples in the literature.[3,5−8] Instead, recent works use the steady-state approach,[9,10] with the downside of supplying the time-average solution of the flow field only.

In the CSTR under consideration, we were interested in examining operating conditions spanning a few decades of the Reynolds number, from the laminar to the fully turbulent regime. We therefore solved the fluid balance equations in the Reynolds-averaged form employing a standard $k - \epsilon$ model to reproduce the effects of turbulent fluctuations. The $k - \epsilon$ model is complemented by the algebraic "law of the wall" to reproduce the turbulent flow up to the near-wall regions. The $k - \epsilon$ model is simple, and its accuracy can be considered comparable to that of more complex turbulence models (renormalization group $k - \epsilon$ models, large eddy simulation models, etc.) provided that the grid is sufficiently refined near the boundaries.[11,12]

In all simulations, we considered a flat upper free surface, i.e., free shear boundary condition, to limit the computational requirements (see discussion in refs 3 and 8).

Table 2. Simulations Performed for Industrial Reactor Equipped with Retreated Curved-Blade Impeller (RCBI) and Turbofoil Turbine (TT)[a]

ref	density (kg/m^3)	viscosity (Pa s)	rpm	*Re*	*Ne*
retreated curved-blade impeller					
R1	10	1	100	30	2.071
R2	1000	5	50	300	0.979
R3	1000	0.001	0.1	3000	0.896
R4	1000	1	100	3000	0.853
R5	1000	0.001 265	50	1 200 000	0.830
R6	1000	0.001	100	3 000 000	0.819
turbofoil turbine					
T1	1000	20	50	60	2.110
T2	1000	1	50	1200	1.075
T3	1000	1.25	100	3000	1.028
T4	1000	0.1	50	12 000	1.035
T5	1000	0.001	50	1 200 000	1.023

[a] Working fluids and operating conditions selected for simulations allow CSTR behavior to be investigated for $Re = 30-(3 \times 10^6)$.

3. Simulations

We performed numerical simulations for the vessel equipped with the RCBI and with the TT over the full range of operating conditions of industrial interest. The operating conditions are characterized by the Reynolds number, defined as

$$Re = \frac{\rho N D^2}{\mu} \tag{1}$$

where ρ and μ are fluid density and viscosity, respectively; D is the impeller diameter; and N is the angular velocity (rpm). Table 2 shows the values of density, viscosity, and angular velocity of the simulations, which span Reynolds numbers in the range $30-(3 \times 10^6)$. In the RCBI simulations, we varied the fluid properties and angular velocities over a wide range, thus ensuring the coherence of the numerical results in the fully turbulent regime. In the TT simulations, we decided to fix the fluid density (1.000×10^3 kg/m^3) and the angular velocity ($N = 50$ rpm), varying the fluid viscosity only. These specific choices do not affect our results because, when the tank size is the same, from similarity theory,[13,14] the Reynolds number is the only parameter relevant for the characterization of the fluid dynamic behavior of a baffled tank. Pairs of simulations R4 and T3 and R5 and T5 were planned to compare in detail the flow fields for the RCBI and the TT. For these simulations, corresponding to $Re = 3000$ and $Re = 1.2 \times 10^6$, respectively, we considered the same fluid density and angular velocity for the RCBI and the TT configurations, and we varied the fluid viscosity slightly to balance the influence of the different impeller diameters in the two configurations.

The simulations required an overall production time, not including grid sensitivity analysis and pre- and postprocessing, of about 60 days of CPU time on our server (two 400-MHz processors, 1 Gb RAM). Long computation times arise from the need to simulate a sufficient number of impeller revolutions to reach the pseudo-steady state. Pseudo-steady state is achieved within 30−40 revolutions in industrial installations, and we needed about 5 h to simulate numerically one complete impeller revolution. To limit the computational effort, we ran trial simulations aimed at verifying the influence of the time step on the accuracy and convergence rate. We found that the optimal time step for the different working conditions depends on the angular velocity of the impeller. For the RCBI, the optimal time step ranges from 0.005 s (for $N = 100$ rpm) to 5 s (for $N = 0.1$ rpm), i.e., each complete impeller revolution requires 120 time steps of simulation. For the TT, the optimal time step ranges from 0.006 s (for $N = 100$ rpm) to 0.012 s (for $N = 50$ rpm), i.e., each complete impeller revolution requires 100 time steps of simulation. Furthermore, we continuously monitored the variation of representative flow variables, namely, the power consumption, the upward flow rate, and the component of momentum in the azimuthal direction, to ensure that the flow field was steady,[3] stopping our analysis as soon as pseudo-steady state was found. Given the computational effort, we limited our analysis to a fixed geometrical configuration for the impellers, corresponding to the value of the off-bottom clearance reported in Table 1.

4. Results

4.1. Power Characteristics. We calculated the power input, P, as the torque on the impeller blades and shaft times the angular velocity[5]

$$P = \boldsymbol{\omega} \cdot \int_A \mathbf{r} \times (\boldsymbol{\tau} \cdot \mathrm{d}\mathbf{A}) \tag{2}$$

where A is the overall impeller and shaft surface, $\boldsymbol{\omega}$ is the angular velocity vector (rps), $\mathbf{r}$ is the position vector, $\boldsymbol{\tau}$ is the stress tensor, and $\mathrm{d}\mathbf{A}$ is the differential surface vector. Then, we represented power consumption by the dimensionless power number, *Ne*, defined as

$$Ne = \frac{P}{\rho N^3 D^5} \tag{3}$$

The results of our calculations for the RCBI and the TT configurations are reported in Table 2.

To validate our results, we considered the power characteristic curve of Nagata.[4] We calculated the parameters of the curve as reported in the Appendix to adapt the power characteristics to our impeller/vessel configurations. It was also possible to measure the power dissipation of the industrial reactor equipped with the RCBI for a single operating condition corresponding to $Re = 2.4 \times 10^6$ and a volume of fluid in the tank equal to 10 000 L. The measured value was $Ne = 0.760$ (accuracy of ±8% in the power consumption) and was estimated by the manifacturer from the power input to the impeller.[15] As discussed in our previous work,[3] this experimental value can be corrected to account for the different volumes of fluid in the tank, i.e., different height-to-tank diameter ratios, H/T. Following Nagata[4] and using eq 12 from the Appendix, we can correct the value up to $Ne = 0.866$. Otherwise, following Armenante and Chang,[16] we can consider that power consumption is independent of the liquid height above the impeller. We compared the experimental value and the experimental value corrected for the H/T ratio with the prediction of the Nagata[4] curve for the RCBI, which is $Ne = 0.780$, and we found a good agreement. Then, we plotted the power characteristics of Nagata,[4] the points calculated by our simulations, and the experimental point for the RCBI configuration, as well as the power characteristics of Nagata[4] and the calculated points for the TT configuration, as shown in Figure 2. First,

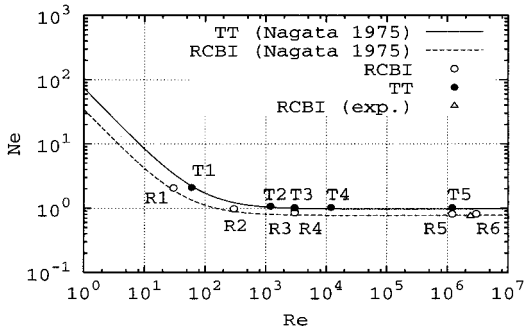

Figure 2. Power number versus Reynolds number: Empirical correlations from Nagata[4] (lines) for industrial-sized vessel equipped with turbofoil turbine (TT) and retreated curved-blade impeller (RCBI) compared to calculated data. An experimental measurement made for the industrial installation (RCBI) is shown for $Re = 2.4 \times 10^6$ (△).

comparing the Nagata[4] curves for the RCBI and the TT configurations, it can be observed that the TT curve predicts power number values larger than the RCBI curve for all values of *Re*. In particular, the increase of *Ne* in the laminar region is steeper for the TT. This finding was in line with our calculations, as shown in Table 2. Second, we considered the points calculated numerically for the TT and RCBI configurations and the corresponding predictions from the Nagata[4] curves, observing that the points fit the curves to a satisfactory degree. In particular, we observed that the computations accurately reproduced the expected Reynolds number power number relation as (i) the transition from laminar to turbulent behavior is captured and (ii) the power number becomes independent of the Reynolds number in the fully turbulent regime, $Re > 10^4$, as shown by the numerical values in Table 2 (R5 and R6 for the RCBI and T4 and T5 for the TT). Finally, we compared the power number value measured in the fully turbulent range for the industrial reactor with the value averaged from simulations R5 and R6, and we were able to estimate that the accuracy of our calculations is within 8.5% in the fully turbulent regime.

4.2. Pumping Capability. We evaluated the stirring produced in the vessel equipped with the RCBI and with the TT by calculating the discharge flow and the circulation flow. The discharge flow, q_d, is defined as

Table 3. Discharge Flow Number and Circulation Flow Number against Reynolds Number for Industrial Reactor Equipped with Retreated Curved-Blade Impeller and Turbofoil Turbine

retreated curved-blade impeller				turbofoil turbine			
Re	N_{qd}	N_{qc}	N_{qc}/N_{qd}[a]	*Re*	N_{qd}	N_{qc}	N_{qc}/N_{qd}[a]
300	0.352	0.363	1.03	60	0.216	0.216	1.
3000	0.451	0.473	1.05	1200	0.339	0.395	1.16
3000	0.435	0.465	1.07	3000	0.374	0.454	1.21
1 200 000	0.345	0.376	1.09	12 000	0.572	0.738	1.28
3 000 000	0.349	0.391	1.12	1 200 000	0.565	0.735	1.30

[a] Discharge flow number to circulation flow number ratio indicates impeller efficiency for entrainment of surrounding fluid.

the flow that crosses the impeller plane. In this work, the discharge flow is calculated by integrating the radial velocity component on the minimal cylindrical surface coaxial with the impeller and enclosing the blades, extending from the bottom of the tank to the height of the impeller tip, as shown in Figure 3. We chose a radius equal to $R = 0.8$ m, i.e., slightly larger than the impeller radius ($R_{imp} = 0.675$ m for the RCBI and $R_{imp} = 0.6$ m for the TT). Judging from the results by Kemoun et al.,[17] this radial distance encloses the potential core of the jet developing from the blade tip. This is the most appropriate choice for the surface over which to calculate the discharge flow, as the impellers examined in this work are radial/axial.

The discharge flow is customarily represented by the dimensionless impeller flow number, or discharge flow number, defined as

$$N_{qd} = \frac{q_d}{ND^3} \tag{4}$$

Table 3 presents the discharge flow numbers calculated for our simulations. For the sake of comparison, we plotted the values of N_{qd} obtained for the RCBI and TT configurations as a function of the Reynolds number, as shown in Figure 4. It can be noted that the discharge flow number peaks in the range 2500−5000 for the RCBI. On a qualitative basis, the pumping capability of the TT is larger than that of the RCBI for $Re > 10^4$ and slightly lower for $Re < 10^4$. The maximum of the

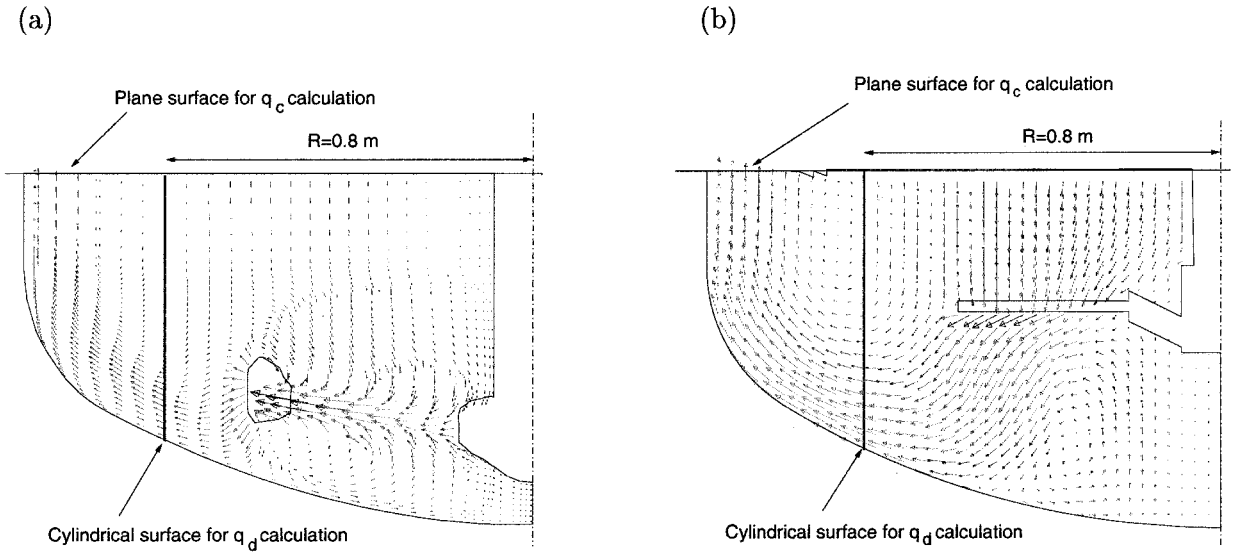

Figure 3. Surfaces used to calculate discharge flow and circulation flow for vessel equipped (a) with a RCBI and (b) with a TT.

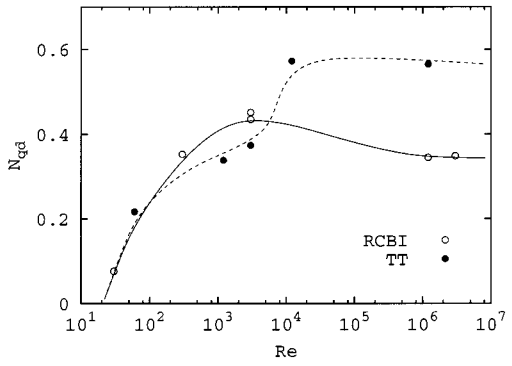

Figure 4. Comparison of discharge flow number for (○) retreated curved-blade impeller and (●) turbofoil turbine.

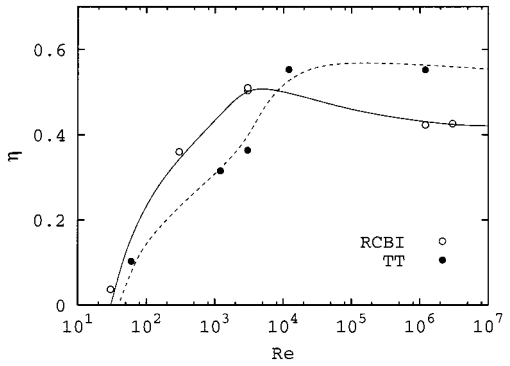

Figure 5. Comparison of efficiency for (○) retreated curved-blade impeller and (●) turbofoil turbine. The turbofoil works better in the high Reynolds number range.

pumping capability is asymptotically found in the fully turbulent regime.

Then, we evaluated the secondary circulation flow, q_c, which is responsible for convective mixing within the tank. The secondary circulation flow is defined as the flux directed upward across a reference section normal to the rotation axis, and it is often used to scale the top−bottom turnover and the mixing time. As shown in Figure 3, for our calculations, we chose the section at the bottom of the cylindrical body of the tank, i.e., near enough to the impeller to observe the variations of the flow field due to the different operating conditions. The secondary circulation flow is customarily represented by the dimensionless secondary circulation flow number, defined as

$$N_{qc} = \frac{q_c}{ND^3} \tag{5}$$

Table 3 shows the values of N_{qc} calculated for the reactor equipped with the RCBI and with the TT. A direct comparison between the values of N_{qc} and N_{qd} offers useful insights into the CSTR fluid dynamic behavior. The discharge flow, q_d, measures the flow rate of the submerged jet generated by the impeller and depends on the impeller geometry and angular velocity. The secondary circulation flow, q_c, is the flow rate of the same jet after interaction with the surrounding fluid. It measures the effectiveness of the jet in transferring motion to the rest of the tank and depends on the vessel configuration (impeller/vessel diameter ratio, number and position of baffles). We calculated the ratio N_{qc}/N_{qd} to evaluate quantitatively the efficiency of this interaction. The values obtained for the vessel equipped with the RCBI and with the TT are presented in Table 3. Simulation R1 was not considered in this analysis because of the different fluid density. A thorough examination of Table 3 suggests that (i) the N_{qc}/N_{qd} ratio is always around unity in the laminar range, (ii) the N_{qc}/N_{qd} ratio progressively increases with the Reynolds number, and (iii) the rate of increase is small for the RCBI and large for the TT. To explain this macroscopic evidence, we examined in detail the structure of three-dimensional flow field generated in the tank by the RCBI and by the TT.

4.3. Pumping Efficiency. We evaluated the efficiency of the RCBI and the TT by calculating the pumping capability per unit of power consumed as

$$\eta = \frac{N_{qd}}{Ne} \tag{6}$$

High efficiency is desired to optimize the balance between the agitation and the costs for agitation. The values obtained for the RCBI and TT configurations are shown in Figure 5 as a function of the Reynolds number. In the RCBI configuration, the pumping efficiency peaks in the range $Re = 2500-5000$ and becomes steady around a value of 0.40 in the fully turbulent regime, corresponding to $Re > 10^4$. In the TT configuration, the value of the pumping efficiency increases and becomes steady around a value of 0.55 for $Re > 10^4$. This trend corresponds to that already observed for N_{qd}. For $Re < 10^4$, the RCBI is capable of generating a larger discharge at lower power compared to the TT. The situation is reversed for $Re > 10^4$, where a given discharge is obtained at a lower power in the TT configuration.

4.4. Flow Field Analysis. To understand the origin of the different macroscopic behavior observed for the RCBI and TT configurations for $Re < 10^4$ and $Re > 10^4$, we examined in detail the fluid dynamics of the flow fields generated by the two impellers. In particular, we examined the flow fields produced by the RCBI and TT for two specific operating conditions, $Re = 3000$ and $Re = 1.2 \times 10^6$. These values of the Reynolds number correspond to conditions for which (i) the efficiencies of the impellers are comparable ($Re = 3000$) and (ii) the efficiency of the TT configuration is larger than that of the RCBI configuration ($Re = 1.2 \times 10^6$). To filter out the influence of blade passage, the flow fields were averaged over one full rotation period, as shown in Figures 6 and 7. In Figure 6a and b, we show the flow fields for $Re = 3000$ for the RCBI and TT configurations, respectively. We represent the radial and axial components of the averaged flow field with vectors and with isocontours of the stream function. We use the same scale for both configurations. It can be observed that the circulation patterns generated by the two impellers are rather different. One of the main reasons for this behavior is the different off-bottom clearance. The velocity vectors suggest that the RCBI generates fluid jets near and almost parallel to the bottom wall. The curved bottom deflects them efficiently, i.e., with low energy dissipation, in the upward direction, giving rise to a large vertical circulation loop. The discharge jets in the TT configuration are generated at greater distances from the bottom and impinge almost normal to the wall. The wall-normal impingement results in substantial kinetic energy dissipation for the jet and, consequently, a reduced velocity. This explains the large values of circulation found for the RCBI configuration compared with the TT configuration for $Re < 10^4$. The lower clearance and the curvature of the tank bottom

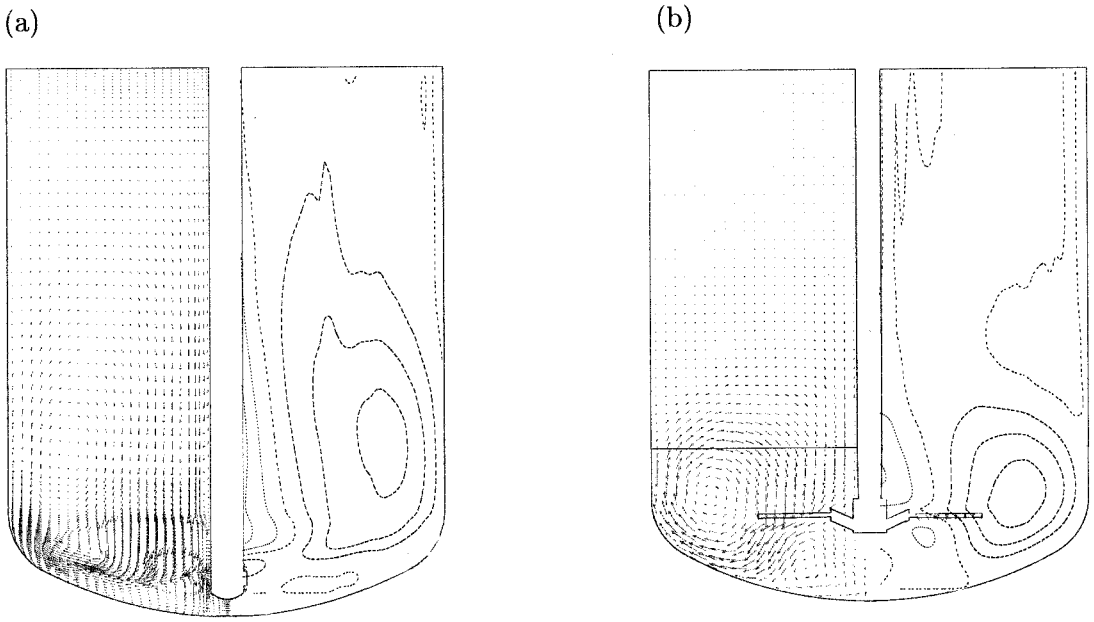

Figure 6. Comparison of flow field generated by retreated curved-blade impeller (left) and turbofoil turbine (right): streamlines and velocity field in a vertical section for $Re = 3000$.

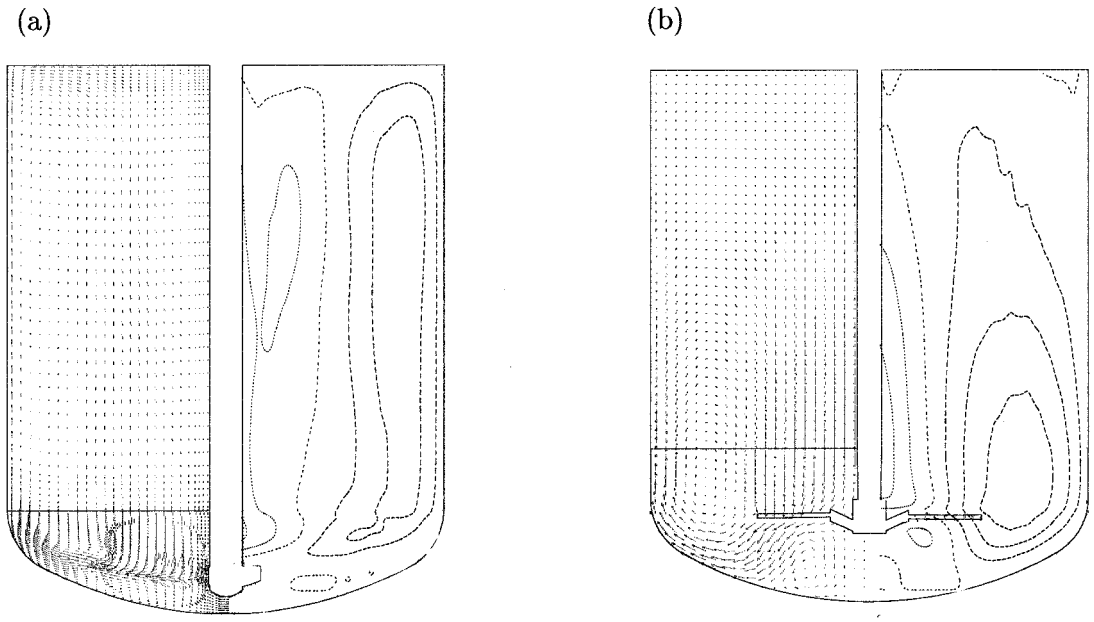

Figure 7. Comparison of flow field generated by retreated curved blade impeller (left) and turbofoil turbine (right): streamlines and velocity field in a vertical section for $Re = 1.2 \times 10^6$.

can also explain the small variation we found for the N_{qc}/N_{qd} ratio in the RCBI configuration as the Reynolds number increases. The lower side of the jet is too near the bottom wall to entrain surrounding fluid. The jet can expand on the upper side only, but it is deflected and rolled up by the curved bottom, thus reducing its possibility to entrain the surrounding fluid. For the TT configuration, the two sides of the jets can generate two circulation loops that are more active than in the RCBI configuration and that develop in an upward direction. However, they remain confined to the lower part of the cylindrical body. This is clearly shown by the streamline contours. Dashed curves and dotted curves represent regions of fluid rotating counterclockwise and clockwise, respectively. The dash-dotted curve is the zero-circulation curve. From Figure 6, it is apparent that, at $Re = 3000$, the ability to generate secondary circulation is larger in the RCBI configuration than in the TT configuration. The wider circulation loop extends up to two-thirds of the vessel height for the field generated by the RCBI and up to one-third of the height for the TT. In Figure 7, the same representation is used for $Re = 1.2 \times 10^6$. In this case, the momentum of the discharge jets of the RCBI is larger than for $Re = 3000$, and the vertical circulation extends to a larger region. The velocity of the TT jets after impingement is still sufficient to extend the circulation loops to the upper part of the vessel. As shown by the streamlines in Figure 7, the flow field in the vertical section is fully developed in the upward direction up to the top of the vessel for both impellers. Nevertheless, the greater graphic density of the streamlines observed in the TT configuration indicates that this impeller generates a larger circula-

Table 4. Dimensionless Geometric Parameters for Industrial Vessel Equipped with Retreated Curved-Blade Impeller and Turbofoil Turbine

	b_{eq}/T	D/T	H/T	B_w/T
RCBI	0.108	0.576	1.33	0.073
TT	0.316	0.51	1.33	0.073

tion flow, as emerges from the previous macroscopic analysis.

5. Conclusions

The objective of this work was to compare the fluid mechanical efficiency of an industrial reactor (nominal capacity of 12 500 L) equipped with two different impellers. This glass-lined reactor is widely used for a number of applications, such as homogeneization, solid suspension, and crystallization, and is equipped with two beaver-tail baffles. We considered two different impellers that can be used to stir the fluid in the vessel, a traditional RCBI and a newer TT, and examined the macroscopic indicators of fluid mechanical efficiency, namely, pumping capability, power consumption, and pumping efficiency. First, we performed three-dimensional, time-dependent numerical simulations of the flow fields generated in the industrial reactor by the two impellers, considering the range of Reynolds numbers of industrial interest. We used the sliding-mesh approach to account for impeller motion. We compared the power consumption calculated by our simulations against the empirical correlation developed by Nagata,[4] obtaining good results. Then, we were able to quantify the discharge flow and the circulation flow generated in the RCBI and TT configurations, as well as the mechanical efficiency. We were able to define the Reynolds number range in which the efficiencies of the RCBI and TT peak, thus providing guidelines for optimized selection of the best impeller/vessel configuration. Finally, we were able to justify, from a microscopic fluid mechanical analysis, the different performances of the two impellers. We found that the off-bottom clearance, and its effect on the discharge jet, might be a first cause of the different fluid dynamic behaviors. Further work is required to evaluate the effects of geometric variables, such as impeller clearance and impeller/vessel diameter ratio, on impeller efficiency.

Acknowledgment

Financial support from MURST under Grant 98093-26392_005 and from Tycon-Technoglass is gratefully acknowledged. We thank in particular Ing. Lorenzo Sassetto and Mr. Gianni Artusi from Tycon-Technoglass for their useful and kind suggestions. Special thanks to Ambra Ambroset and Alessandro Agosto for performing some numerical simulations.

Appendix

Empirical Correlations. The general form of the power characteristic (see Nagata[4]) is

$$Ne = \frac{A}{Re} + B\left(\frac{10^3 + 0.6f\,Re^{\alpha}}{10^3 + 1.6f\,Re^{\alpha}}\right)^{p} \tag{7}$$

The first term represents power consumption in the laminar range, and the second term indicates power consumption in the turbulent range. Coefficients of the empirical equation A, B, p, f, and α are estimated from the geometrical characteristics of the CSTR using correlations derived experimentally from data collected for a simple configuration (single-paddle impeller, $H/T = 1$, vertical blades, $\theta = 90°$)

$$A = 14 + \frac{b}{T}\left[670\left(\frac{D}{T} - 0.6\right)^2 + 85\right] \tag{8}$$

$$B = 10^{[1.3 - 4(b/T - 0.5)^2 - 1.14D/T]} \tag{9}$$

$$p = 1.1 + 4\left(\frac{b}{T}\right) - 2.5\left(\frac{D}{T} - 0.5\right)^5 - 7\left(\frac{b}{T}\right)^4 \tag{10}$$

$$f = 2 \qquad \alpha = 0.66 \tag{11}$$

Corrections are needed for CSTRs with different configurations:

1. Effect of Different Number of Paddles and Different Impeller Type. An equivalent blade height $b_{eq} = bn_p$, is used instead of b in eqs 8−11. The number of paddles, n_p, is calculated from the number of blades. Each blade is equivalent to 0.5 paddles.

2. Effect of Liquid Depth. A multiplicative factor C is used for the turbulent contribution to power consumption

$$C = \left(\frac{H}{T}\right)^{0.35 + b/T} \tag{12}$$

3. Effect of Blade Inclination. A multiplicative factor C_1 is used for the turbulent contribution to power consumption

$$C_1 = (\sin\theta)^{1.2} \tag{13}$$

4. Effect of Baffles. Geometrical characteristics of the baffles are used to determine the asymptotic value for power dissipation, corresponding to (a) "fully baffled" conditions

$$\left(\frac{B_w}{T}\right)^{1.2} n_B = 0.35 \tag{14}$$

which imply maximum power consumption, Ne_{max}, given by

$$Ne_{max} = \frac{A}{Re} + BC \tag{15}$$

(b) partially baffled conditions, which imply a power number, Ne_B, given by

$$\frac{Ne_{max} - Ne_B}{Ne_{max} - Ne_\infty} = \left[1 - 2.9\left(\frac{B_w}{T}\right)^{1.2} n_B\right]^2 \tag{16}$$

Table 5. Correlation Parameters for Examined Configurations

	A	B	p	C	Ne_∞	Ne_{max}	Ne_{max}/Ne_∞	Ne_B/Ne_∞
industrial CSTR (RCBI)	34.02	1.068	1.532	1.139	0.237	1.217	5.135	2.86
industrial CSTR (TT)	74.10	3.825	2.293	1.212	0.404	4.624	11.44	5.55

where Ne_∞, the power number obtained for Re tending to infinity, is given by

$$Ne_\infty = B\left(\frac{0.6}{1.6}\right)^p \tag{17}$$

Corrections factors are used to represent the following curves:

1. the "no baffle" curve

$$Ne = \frac{A}{Re} + B\left(\frac{10^3 + 0.6f\,Re^\alpha}{10^3 + 1.6f\,Re^\alpha}\right)^p \tag{18}$$

2. the "baffled" curve

$$Ne = \frac{A}{Re} + BCC_1 \cdot \frac{Ne_B}{Ne_\infty}\left(\frac{10^3 + 0.6f\,Re^\alpha}{10^3 + 1.6f\,Re^\alpha}\right)^p \tag{19}$$

3. the "fully baffled" curve

$$Ne = \frac{A}{Re} + B\frac{Ne_{max}}{Ne_\infty}\left(\frac{10^3 + 0.6f\,Re^\alpha}{10^3 + 1.6f\,Re^\alpha}\right)^p \tag{20}$$

Table 4 shows dimensionless geometric parameters derived for the configurations examined. These values were used to calculate the correlation parameters shown in Table 5, from which we derived the functional representations of the power characteristics.

Literature Cited

(1) Verschuren, I.; Wijers, J.; Keurentjes, J. Mixing in a Pfaulder type impeller: The effect of micromixing on reaction selectivity in the production of fine chemicals. In *Proceedings of the 10th European Conference on Mixing*; Elsevier: Amsterdam, 2000; p 69.

(2) Schafer, M.; Yu, J.; Genenger, B.; Durst, F. Turbulence generation by different types of impellers. In *Proceedings of the 10th European Conference on Mixing*; Elsevier: Amsterdam, 2000; p 9.

(3) Campolo, M.; Paglianti, A.; Soldati, A. Fluid dynamic efficiency and scale-up of a retreated blade impeller CSTR. *Ind. Eng. Chem. Res.* **2002**, 41, 164.

(4) Nagata, S. *Mixing: Principles and Applications*; Kodansha: Tokyo, Japan, 1975.

(5) Harvey, A. D.; Rogers, S. E. Steady and unsteady computation of impeller stirred reactor. *AIChE J.* **1996**, *42*, 2701.

(6) Brucato, A.; Ciofalo, M.; Grisafi, F.; Micale, G. Numerical prediction of flow fields in baffled stirred vessel: A comparison of alternative modelling approaches. *Chem. Eng. Sci.* **1998**, *53*, 3654.

(7) Schafer, M.; Yianneskis, M.; Wachter, P.; Durst, F. Trailing vortices around a 45° pitched blade impeller. *AIChE J.* **1998**, *44*, 1233.

(8) Serra, A.; Campolo, M.; Soldati, A. Time-dependent finite-volume simulation of the turbulent flow in a free-surface CSTR. *Chem. Eng. Sci.* **2001**, *56*, 2715.

(9) Harvey, A. D.; Lee, C. K.; Rogers, S. E. Steady-state modeling and experimental measurement of a baffled impeller stirred tank. *AIChE J.* **1995**, *41*, 2177.

(10) Wechsler, K.; Breuer, M.; Durst, F. Steady and unsteady computations of turbulent flow induced by a 4/45° pitched-blade impeller. *J. Fluids Eng.* **1999**, *121*, 318.

(11) Bartels, C.; Breuer, M.; Durst, F. Comparison between direct numerical simulation and $k-\epsilon$ prediction of the flow in a vessel stirred by a Rushton turbine. In *Proceedings of the 10th European Conference on Mixing*; Elsevier: Amsterdam, 2000; p 239.

(12) Ranade, V. V.; Joshi, J. B.; Marathe, A. G. Flow generated by pitched blade turbines. II: Simulation using $k-\epsilon$ model. *Chem. Eng. Commun.* **1989**, *81*, 225.

(13) Rushton, H. J. Applications of fluid mechanics and similitude to scale-up problems. Part 1. *Chem. Eng. Prog.* **1952**, *48*, 33.

(14) Rushton, H. J. Applications of fluid mechanics and similitude to scale-up problems. Part 2. *Chem. Eng. Prog.* **1952**, *48*, 95.

(15) Sassetto, L.; Artusi, G. Tycon-Technoglass, Quarto d'Altino, Venice, Italy. Personal comunication, 2000.

(16) Armenante, P. M.; Chang, G. M. Power consumption in agitated vessels provided with multiple-disk turbines. *Ind. Eng. Chem. Res.* **1998**, *37*, 284.

(17) Kemoun, A.; Lusseyran, F.; Mallet, J.; Mahouast, M. Experimental scanning for simplifying the model of a stirred-tank flow. *Exp. Fluids* **1998**, *25*, 23.

Received for review June 27, 2001
Revised manuscript received November 13, 2001
Accepted November 21, 2001

IE010561E